P2-type $Na_{2/3}Ni_{1/3}Mn_{2/3}O_2$ Cathode Material with Excellent Rate and Cycling Performance for Sodium-Ion Batteries

Jing Mao,[1,2] Xin Liu,[1,2] Jianwen Liu,[3] Heyang Jiang,[3] Tao Zhang,[1.4] Guosheng Shao,[1,2] Guo Ai,[5,6] Wenfeng Mao,[7] Yan Feng,[7] Wanli Yang,[8] Gao Liu,[9,z] and Kehua Dai[3,7,z]

[1]School of Materials Science and Engineering, Zhengzhou University, Zhengzhou 450001, China

[2]International Joint Research Laboratory for Low-Carbon & Environmental Materials of Henan Province, Zhengzhou University, Zhengzhou 450001, China

[3]School of Metallurgy, Northeastern University, Shenyang 110819, China

[4]Zhengzhou Institute of Emerging Industrial Technology, Zhengzhou 450001, China

[5]College of Physics and Materials Science, Tianjin Normal University, Tianjin 300387, China

[6]Science and Technology on Reliability Physics and Application of Electronic Component Laboratory, No. 5 Electronic Research Institute of the Ministry of Industry and Information Technology, Guangzhou 510610, China

[7]College of Chemistry, Tianjin Normal University, Tianjin 300387, China

[8]Advanced Light Source, Lawrence Berkeley National Laboratory, Berkeley, California 94720, USA

[9]Energy Storage and Distributed Resources Division, Energy Technologies Area, Lawrence Berkeley National Laboratory, Berkeley, California 94720, USA

[z]E-mail: daikh@smm.neu.edu.cn; gliu@lbl.gov

Abstract: P2-type $Na_{2/3}Ni_{1/3}Mn_{2/3}O_2$ is an air-stable cathode material for sodium-ion batteries. However, it suffers irreversible P2-O2 phase transition in 4.2-V plateau and shows poor cycling stability and rate capability within this plateau. To evaluate the practicability of this material in 2.3-4.1 V voltage range, single-crystal micro-sized P2-type $Na_{2/3}Ni_{1/3}Mn_{2/3}O_2$ with high rate capability and cycling stability is synthesized via polyvinylpyrrolidone (PVP)-combustion method. The electrochemical performance is evaluated by galvanostatic charge-discharge tests. The kinetics of Na^+ intercalation/ deintercalation is studied detailly with potential intermittent titration technique (PITT), galvanostatic intermittent titration technique (GITT) and cyclic voltammetry (CV). The discharge capacity at 0.1 C in 2.3-4.1 V is 87.6 mAh g^{-1}. It can deliver 91.5% capacity at 40 C rate and keep 89% after 650 cycles at 5C. The calculated theoretical energy density of full cell with hard carbon anode is 210 Wh kg^{-1}. The moderate energy density associated with high power density and long cycle life is acceptable for load adjustment of new-energy power, showing the prospect of practical application.

1. Introduction

In recent years, sodium-ion batteries have been paid more and more attentions by researchers due to the high demand of resources for large-scale applications such as

electric vehicles and energy storage[1-8]. Layered transition metal oxides (TMO) are promising competitors in practical cathode materials for sodium ion batteries due to their convenient synthesis, simple structure and abundant resources[9-11]. Xiang and Chen et al. point out that TMO materials have high energy density and large space to improve cycling and rate performance, so they are the most promising cathode materials for sodium-ion batteries[6].

The TMO materials for sodium-ion batteries have two main structures: P2- and O3-type structures[7]. Comparatively, P2 structure has better rate performance because sodium ions are located in the prismatic sites and can easily migrate to the adjacent sites[9]. On the contrary, sodium ions in O-type structure are in octahedral sites, then their migration must go through tetrahedral sites. Because of the large volume of sodium ions, this migration barrier is relatively high, resulting relatively poor rate capability for O-type structure. Considering this, we focus on P2-type TMOs in this paper. Among the P2-type TMOs, manganese-based sodium transition metal oxides, $Na_yMn_{1-x}M_xO_2$ (x, y ≤ 1, M = Ni, Fe, Co, Ti, Cu, Mg, Li, etc.), have been widely studies[12-18]. However, the rate capability and cycling stability of them are still unsatisfied. In addition, many of $Na_yMn_{1-x}M_xO_2$ are not stable in air due to the Jahn–Teller active Mn^{3+}[19]. These disadvantages hinder the application of these materials.

P2-type $Na_{2/3}Ni_{1/3}Mn_{2/3}O_2$ is an air-stable compound because the Mn is +4 valence while Ni is +2 valence[20, 21]. It was firstly reported by Dahn's group in 2001[22]. The initial discharge capacity of this material in 1.6-4.5 V voltage range is over 200 mAh g^{-1} but the cycling stability and rate capability are very poor due to the irreversible

P2-O2 phase transition and sluggish kinetic in the 4.2-V plateau[23]. A recent study points out there may be poorly reversible oxygen activities in this plateau which causes capacity decay[24]. To improve, Liu et al. reported an Al_2O_3 coated $Na_{2/3}Ni_{1/3}Mn_{2/3}O_2$ that shows ~160 mAh g^{-1} initial discharge capacity in 2.5-4.3 V range and keeps 73.2% after 300 cycles[25]. The Al_2O_3 coated $Na_{2/3}Ni_{1/3}Mn_{2/3}O_2$ shows improved but still limited rate capability, e.g. 120 mAh g^{-1} at 1C. Risthaus et al. improved the cycling stability of $Na_{2/3}Ni_{1/3}Mn_{2/3}O_2$ by optimizing electrolyte component and additive[24]. Another solution is limiting voltage cut-off to avoid P2-O2 transition. Shirley Meng's group greatly enhanced the cycling stability through shrinking cut-off voltages to 2.3-4.1 V[23]. The $Na_{2/3}Ni_{1/3}Mn_{2/3}O_2$ exhibits stable cycling with initial discharge capacity of 82 mAh g^{-1} and capacity retention after 50 cycles of 92%, although the rate capability is still not satisfied. For such a relatively small capacity (80~90 mAh g^{-1}), this material must be endowed with some highlights before it can be applied. We believe that super high rate capability can compensate the shortage of capacity.

Previously, we reported a polyvinylpyrrolidone (PVP)-combustion method. With this method, we prepared some TMO materials for Li-ion and Na-ion batteries with high rate capability and cycling stability[26-30]. PVP can fix metal ion on the macromolecular chain via chelation, so the precursor is very uniform which benefits good electrochemical performance. In this paper, we prepared P2-type $Na_{2/3}Ni_{1/3}Mn_{2/3}O_2$ with high rate capability and cycling stability by this method and discussed its practical prospect.

2. Experimental

2.1 Material synthesis

$Na_{2/3}Ni_{1/3}Mn_{2/3}O_2$ was prepared by PVP-combustion method. Stoichiometric $NaOAc{\cdot}4H_2O$, $Ni(OAc)_2{\cdot}4H_2O$ and $Mn(OAc)_2{\cdot}4H_2O$, and PVP (the molar ratio of PVP monomer to total metal ions was 2.0) were dissolved in deionized water and pH = 3 was achieved by adding 1:1 HNO_3. The mixture was stirred at 120 °C to obtain dried gel. The dried gel was ignited on a hot plate to induce a combustion process which lasted for several minutes. The resulting precursor was preheated at 400 °C for 2 h and then calcined at 1000 °C for 6 h with the heating rate of 5 °C min^{-1}. After heat treatment, the oven was switched off and the sample was cooled down naturally. The whole process was performed in air.

2.2 Physical characterization

The morphology was examined using a JEOL 7500F scanning electron microscope (SEM). The analysis of the phase purity and the structural characterization were made by X-ray powder diffraction (XRD) using a Bruker D2 PHASER diffractometer equipped with Cu Kα radiation. Soft x-ray absorption spectroscopy (sXAS) was performed in the iRIXS endstation at Beamline 8.0.1 of the Advanced Light Source (ALS) at LBNL. All the sXAS spectra have been normalized to the beam flux measured by the upstream gold mesh. The experimental energy resolution is 0.15 eV without considering core-hole lifetime broadening.

2.3 Electrochemical tests

The $Na_{2/3}Ni_{1/3}Mn_{2/3}O_2$ cathode was prepared by mixing 80 wt.% active material, 10 wt.% acetylene black (AB) and 10 wt.% polyvinylidene fluoride (PVdF) binder in N-methylpyrrolidone (NMP) to form a slurry. The slurry was doctor-bladed onto aluminum foil, dried at 60 °C, and then punched into electrode discs with a diameter of 12.7 mm. The prepared electrodes were dried at 130 °C for 12 h in a vacuum oven and show typically an active material loading of about 4 mg cm^{-2}. The electrochemical cells were fabricated with the $Na_{2/3}Ni_{1/3}Mn_{2/3}O_2$ cathode, sodium foil anode, 1 mol L^{-1} $NaClO_4$ in propylene carbonate (PC) as electrolyte, and double layered glass fiber as separator in an argon-filled glove box. Electrochemical performances were evaluated using CR2325 coin cells. The galvanostatic charge-discharge tests were performed using Maccor 4000. The galvanostatic intermittent titration technique (GITT) test, potential intermittent titration technique (PITT) test and cyclic voltammetry (CV) measurements were conducted using Bio-Logic VMP-3 multichannel electrochemical Analyzer. In the PITT test, a small potential step size (10 mV) and a low enough cutoff current (C/50) were adopted to ensure the equilibrium states were achieved at every potential step. All the cells keep 30 °C during electrochemical tests.

3. Results and discussion

3.1 Structure and morphology

As shown in Fig. 1a, the XRD pattern of the as-prepared $Na_{2/3}Ni_{1/3}Mn_{2/3}O_2$

confirms the formation of well crystallized material. All the diffraction peaks can be labeled as hexagonal P2-type structure and $P6_3/mmc$ space group[20, 22, 31]. Fig. 1b&c shows the SEM image and corresponding calculated particle size distribution of the well-crystallized $Na_{2/3}Ni_{1/3}Mn_{2/3}O_2$. The morphology is smooth-faced without secondary-particle structure. The particle size distribution is between 1 μm and 5 μm and mean size is 2.2 μm which is counted from 200 particles in a lower magnification SEM image. Such morphology is not only good for high tap-density but also generally desirable for improving the cycling stability due to lower side reactions. Moreover, it is believed that this single-crystal morphology without significant grain boundaries and defects could facilitate ionic diffusion and then could improve rate capability[27].

Mn and Ni oxidation states in the as-prepared $Na_{2/3}Ni_{1/3}Mn_{2/3}O_2$ are studied by soft X-ray absorption spectroscopy (sXAS), which is performed at the Advanced Light Source (ALS) and shown in Fig. 2 with Mn^{4+} and Ni^{2+} standard spectra. Mn and Ni *L*-edge sXAS spectra directly probes the electron dipole transition from 2*p* core level to the 3*d* valence states[32-36]. Both TEY (total electron yield, surface sensitive) and TFY (total fluorescence yield, bulk sensitive) L_3-edge spectra of Mn and Ni highly agree with Mn^{4+} and Ni^{2+} standard spectra, respectively. The larger t_{2g} (lower energy peak) and e_g (higher energy peak) split of as-prepared $Na_{2/3}Ni_{1/3}Mn_{2/3}O_2$ than that of calculated Ni^{2+} is due to stronger crystal field in this material. Thus, the Mn and Ni valence in this as-prepared material is +4 and +2, respectively.

3.2 Charge and discharge profiles at low rate

The theoretical initial specific charge and discharge capacity of $Na_{2/3}Ni_{1/3}Mn_{2/3}O_2$

is 173 and 259 mAh g^{-1} assuming 2/3 and 1 mol Na^+ be transferred, respectively. For this as-prepared $Na_{2/3}Ni_{1/3}Mn_{2/3}O_2$, the initial charge profile at 0.1C shown in Fig. 3a can be divided to three plateaus in general: 3.3 V, 3.7 V and 4.2 V. The specific capacity and Na transfer amount of the three plateaus are 41, 44, 80 mAh g^{-1} and 0.16, 0.33, 0.31 mol (calculated by Faraday's constant and molar mass, assuming all the capacity are contributed by Na^+ transfer), respectively. The corresponding *x* values in $Na_xNi_{1/3}Mn_{2/3}O_2$ after these plateaus are 0.51, 0.34 and 0.03. These values are very close to the calculation [23], showing the perfect structure obtained by the PVP-combustion method.

The structure keeps P2 type before 4.0 V and the 3.3-V and 3.7-V plateaus are considered as in-plane ordering transfer [23]. Lu and Dahn [22] consider the sharp steps at $x = 2/3$, $x = 1/2$, and $x = 1/3$ may correspond to the composition of phases with ordered arrangements of intercalant. During the long and flat 4.2-V plateau with ~1/3 Na^+ extracted, the structure suffers P2-O2 phase change [23]. During this P2-O2 phase change, the central MO_2 sheet glides in the a-b plane, which causes stacking faults because there are two choices for the slide direction. Thus, the charging and discharging process involving 4.2-V plateau should show poor reversibility and sluggish kinetics. In a recent work, Risthaus et al. [24] point out that oxygen redox involved at this stage through O-*K* edge XAS. This provides a new insight to understand the unsatisfied electrochemical performance of the 4.2-V plateau. However, as we pointed out previously [37-40], sXAS is unreliable for studying oxygen redox but mRIXS is an ideal tool to fingerprint it in battery electrodes. Quantitative

study of oxygen redox in this material will be shown in further works.

$$NaNi_{\frac{1}{3}}Mn_{\frac{2}{3}}O_2 \overset{\frac{1}{3}Na,\ 1.8\ V}{\longleftrightarrow} Na_{\frac{2}{3}}Ni_{\frac{1}{3}}Mn_{\frac{2}{3}}O_2 \overset{\frac{1}{6}Na,\ 3.3\ V}{\longleftrightarrow} Na_{\frac{1}{2}}Ni_{\frac{1}{3}}Mn_{\frac{2}{3}}O_2$$

$$\overset{\frac{1}{6}Na,\ 3.7\ V}{\longleftrightarrow} Na_{\frac{1}{3}}Ni_{\frac{1}{3}}Mn_{\frac{2}{3}}O_2 \overset{\frac{1}{3}Na,\ 4.2\ V}{\longleftrightarrow} Na_0Ni_{\frac{1}{3}}Mn_{\frac{2}{3}}O_2 \quad (1)$$

In the discharging process to 1.5 V, a new 1.8 V plateau comes up besides the three plateaus discussed above, which leads to a high discharge capacity of 221 mAh g^{-1}, corresponding to $Na_{0.89}Ni_{1/3}Mn_{2/3}O_2$ at fully discharged state. In a summary, the charge and discharge process of $Na_{2/3}Ni_{1/3}Mn_{2/3}O_2$ can be approximatively explained in eq. (1).

Fig. 3b shows the CV curves with a 0.05 mV s^{-1} scan speed between 1.5 and 4.4 V. All the redox peaks in CV agree with the charge and discharge profiles. Generally speaking, the reversibility in 3-4 V is better than that below 3 V and above 4 V. This suggests the thermodynamic is more reversible and/or the kinetics is faster in 3-4 V.

3.3 Rate capability and kinetics of Na^+ intercalation/deintercalation

Rate capability of the as-prepared $Na_{2/3}Ni_{1/3}Mn_{2/3}O_2$ is measured by both normal and fast tests, which are shown in Fig. 4a to 4c. Fast rate test method was developed by Newman *et al.* [41] The mechanism and procedure of fast rate tests were discussed in our previous work[28]. As shown in Fig. 4b, the cell is discharged at 40 C to 2.0 V, then after 5-min rest, the cell's voltage is about 3.2 V, afterwards it is discharged at 20 C. In the same way, the rest and discharge alternate at 10 C, 5 C, 2 C, 1C, C/2 and C/5. The capacity during 40 C discharge plus that during 20 C is considered as the capacity for 20 C. The "40 C + 20 C +10 C" capacity is the capacity for 5 C, and so on. Both normal and fast tests suggest the rate capability of this material in 2.3-4.1 V is much

better than previous reports (see Table 1). The discharge capacity in 2.3-4.1 V at 0.1 C and 5 C are 87.6 mAh g^{-1} and 83.6 mAh g^{-1} with normal rate test, respectively. The ratio of 5 C/0.1 C is 95.4%, namely, the discharge capacity decreases only a little from 0.1 C to 5 C. The ratio of 40 C/0.1 C is 91.5% with fast rate test, showing superior high-rate capability in 2.3-4.1 V. While the rate capability in 1.5-4.1 V and 2.3-4.5 V (see Fig. S1 and S2) are not as good as that in 2.3-4.1 V due to the possible sluggish kinetics in 1.8 V and 4.2 V plateau, the results agree with previous data[25, 42, 43].

To further understand the kinetics of Na^+ intercalation/deintercalation, the Na^+ diffusion coefficient is measured by cyclic voltammetry (CV) and potentiostatic intermittent titration technique (PITT) tests. The methods and calculation procedures are described in our previous works [27, 28]. In the PITT experiments, the sodium chemical diffusion coefficient, D_{Na^+}, can be calculated from the slope of the linear region in the ln $I(t)$ *vs.* t plot, as defined in equation (2):

$$D_{Na^+} = -\frac{d\ln(I)}{dt}\frac{4L^2}{\pi^2} \quad (2)$$

where I is the current in the potential step and L is the diameter of a spherical particle. Fig. 4e and 4f show the calculated D_{Na} values from PITT method at different Na^+ intercalation/deintercalation stage. In the charging process, the Na^+ diffusion coefficient in the 3.3-V and 3.7-V plateaus is about 10 times higher than that in 4.2-V plateau. Similarly, in the discharging process, the coefficient in the 3.3-V and 3.7-V plateaus also about 10 times higher than that in 4.1-V and 1.8-V plateau, explaining the much better rate capability in 2.3-4.1 V than it in 1.5-4.1 V or 2.3-4.5 V range.

In the CV test, for a reversible reaction relating Na^+ ion diffusion behavior, the

sodium chemical diffusion coefficient (D_{Na^+}) can be determined on the basis of the following Randles-Sevcik equation:

$$i_p = 0.4463 n^{\frac{3}{2}} F^{\frac{3}{2}} C_{Na} A R^{-\frac{1}{2}} T^{-\frac{1}{2}} D_{Na}^{\frac{1}{2}} v^{\frac{1}{2}} \quad (3)$$

At 30 °C:

$$i_p = (2.67 \times 10^5) n^{\frac{3}{2}} C_{Na} A D_{Na}^{\frac{1}{2}} v^{\frac{1}{2}} \quad (4)$$

where i_p is the peak current value (A), n is the number of electrons per reaction species (for Na^+ n = 1), C_{Na} is the bulk concentration of lithium-ion in the electrode (0.024 mol cm^{-3}), A is the surface area of electrode (here is 1.26 cm^2), D_{Na} is the sodium chemical diffusion coefficient (cm^2 s^{-1}), and v is the scan rate (V s^{-1}). The CV tests are run from 2.3 V to 4.1 V, the scan rates in the start 3 cycles are 0.05 mV s^{-1}, 0.2 mV s^{-1} and 0.5 mV s^{-1}, respectively. After that, the scan rate keeps 0.5 mV s^{-1} for 20 cycles. The cell rests 2 h for balance between different cycles. The high repeatability of the different cycles in Fig. 4d suggests a reversible reaction relating Na^+ ion diffusion behavior, so the equation (4) could be used to calculate D_{Na}. From the slope of linear fit of the peak current (i_p) vs. the square root of the scan rates ($v^{½}$), the calculated D_{Na} of 3.7-V oxidation peak is 3.5×10^{-10} cm^2 s^{-1}. This value is roughly consistent with PITT results (the average value of four points around the 3.7-V plateau is 2.9×10^{-10} cm^2 s^{-1}), suggesting very fast Na^+ intercalation kinetics of this material.

With the calculated sodium diffusion coefficient, the diffusion time of Na^+ in the particles can be estimated by $L^2 = Dt$. The mean particle size is 2.2 μm, so $L^2 = 4.8 \times 10^{-8}$ cm, t ≈ 2 min. This could roughly explain the high discharge capacity at 40 C

(discharging time is 1.5 min). On the other hand, the diffusion coefficient determines the upper limit of rate capability. In a half cell, the rate capability is also affected by electrode structure, contact of battery component, separator and electrolyte. For example, the sodium diffusion coefficient in this work is similar with some previous reports [23, 31], but our rate capability is much higher than them. This may be explained by the uniform single-crystal morphology in this work which can improve the homogeneity of cathode material and conductive additive.

Overpotential is another important data for kinetics of Na^+ intercalation/ deintercalation besides sodium diffusion coefficient. Overpotential can interpret the electrode polarization and be used to estimate irreversible heat generation which is important for batteries safety [44]. This has never been studied in $Na_{2/3}Ni_{1/3}Mn_{2/3}O_2$. Galvanostatic intermittent titration technique (GITT) is usually used to anylysis overpotential. As shown in Fig. 5a, the voltage profile of GITT is composed of galvanostatic charging or discharging and relax alternately. The charging or discharging rate is 0.1 C, each charging or discharging step is 10-min long or until cut-off voltage, and each relax step is 40-min long or until $|dV/dt| < 1$ mV min^{-1}. Fig. 5b exhibits a typical potential response within the GITT test as well as the definition of the IR-drop, η_{IR}, and the overpotential due to mass transport limitation, η_D. The IR-drop is due to both ohmic resistance and the charge transfer at the electrolyte-electrode interface. The η_D is caused by mass transport limitations and depends on x in $Na_xNi_{1/3}Mn_{2/3}O_2$ [44].

Fig. 5c and 5d show the η_{IR} and η_D during charging and discharging in the 1st and 2nd

cycles. The η_{IR} and η_D values at same x value are rather different in charging (desodiation) and discharging (sodiation). The η_D and η_{IR} values are generally low in the initial charging except some points. The η_D and η_{IR} values at plateau 1 in the discharging are both higher than the values in charging while the η_D values at plateau 3 in the discharging are much higher than the values in charging. In the 2nd cycle, the η_D values become higher in the start of charging, and the η_D values at plateau 3 in the discharging are higher than the values in the 1st cycle. Nevertheless, the η_D and η_{IR} values at plateau 1 and 2 are similar with those in 1st cycle. These results indicate that plateau 3 has poor reversibility and cyclability. Fig. 5e and 5f show η_{IR} and η_D values at different plateau during cycling. The η_{IR} and η_D at charging plateau 1&2 and discharging plateau 1 change very little during cycling. In the contrary, the η_D at plateau 3 (both charging and discharging) increase greatly during cycling, and the η_D at plateau 3 in discharging become to increase after 5 cycles. These results suggest the mass transport limitation increase is the main factor of the overpotential increase during cycling. The increase of η_D in discharging also explains why fast rate test method can give intrinsic rate capability results: the mass transport limitation increases along with cycling, and normal rate test usually needs several cycles, but the fast rate test only need 1 cycle.

3.4 Cycling stability

Although the capacity retention in 1.5-4.1 V is 60% after 300 cycles and that in 1.5-4.5 V is even much lower (see Fig. S3), the as-prepared $Na_{2/3}Ni_{1/3}Mn_{2/3}O_2$ shows very excellent cycling stability in 2.3-4.1 V range. Fig. 6a and 6b show that the

capacity retention is 94% and 69% in 2.3-4.1 V at 1C after 300 and 900 cycles, respectively. This is consistent with the CV test in Fig. 4d, in which the curves coincide well at different cycles. The coulombic efficiency is close to 100% during 1C cycling. As shown in Fig. 6c, at 5C high rate, this material also shows very stable cycling in 2.3-4.1 V with an 89% capacity retention after 650 cycles. The much better cycling stability in 2.3-4.1 V than that in 1.5-4.1 V or 1.5-4.5 V is benefited by avoiding P2-O2 phase change [23] and the formation of Mn^{3+}[24].

As shown in table 1, the as-prepared $Na_{2/3}Ni_{1/3}Mn_{2/3}O_2$ shows the best cycling performance compared with previous reports. The excellent cycling stability might be attributed to: i) The PVP-combustion method. The remarkable advantages of PVP-assisted combustion method over other polymer-pyrolysis methods has been discussed previously[32]. PVP helps a homogeneous distribution of the constituents at the atomic level and improves the crystallization, purity and homogeneity of $Na_{2/3}Ni_{1/3}Mn_{2/3}O_2$[26-28, 32, 45]. ii) The uniform single-crystal morphology and appropriate particle size. The smooth single-crystal morphology could suppress side reactions. The particle size is both not too small (mostly higher than 1 μm) and not too big (mostly lower than 4 μm), possibly preventing metal ion solution and cracks which occur on the surface of big particles[46].

4. Conclusions

$Na_{2/3}Ni_{1/3}Mn_{2/3}O_2$ with ultra-high rate capability and excellent cycling stability in 2.3-4.1 V range is synthesized via PVP-combustion method. The comprehensive

electrochemical performance is improved compared with previous reports which are shown in Table 1. The discharge capacity is 87.6 mAh g^{-1} at 0.1 C rate in 2.3-4.1 V. This capacity is comparable with $Li_{1+x}Mn_{2-x}O_4$ material [47], and the theoretical energy density of full cell with hard carbon anode [48] (reversible capacity is 370 mAh g^{-1}) is 210 Wh kg^{-1} (average voltage of full cell is 3.0 V). Moreover, this material can deliver 91.5% capacity at 40 C rate and keep 89% after 650 cycles at 5C. The moderate energy density associated with high power density and long cycle life is acceptable for load adjustment of new-energy power, showing the prospect of practical application[8].

The kinetics of Na^+ intercalation/deintercalation is studied detailly with PITT, GITT and CV. The Na^+ diffusion coefficient in the 3.3-V and 3.7-V plateaus is about 10 times higher than that in 4.2-V plateau. The CV test indicates the D_{Na} of 3.7-V oxidation peak is 3.5×10^{-10} cm^2 s^{-1}. The GITT tests show the mass transport limitation increase is the main factor of the overpotential increase during cycling.

Acknowledgements

We acknowledge the support from the National Natural Science Foundation of China (51604244), Postdoctoral research grant in Henan province (001802003), Science and Technology on Reliability Physics and Application of Electronic Component Laboratory open fund (ZHD201605) and Assistant Secretary for Energy Efficiency and Renewal Energy under the Battery Materials Research (BMR) program under Contract No. DE-AC02-05CH11231. This research used resources of the Advanced

Light Source, which is a DOE Office of Science User Facility under contract no. DE-AC02-05CH11231.

References

1. E. A. Olivetti, G. Ceder, G. G. Gaustad and X. Fu, *Joule*, **1**, 229 (2017).

2. M. D. Slater, D. Kim, E. Lee and C. S. Johnson, *Adv. Funct. Mater.*, **23**, 947 (2013).

3. H. Kim, H. Kim, Z. Ding, M. H. Lee, K. Lim, G. Yoon and K. Kang, *Adv. Energy Mater.*, **6**, 38 (2016).

4. K. Kubota and S. Komaba, *J. Electrochem. Soc.*, **162**, A2538 (2015).

5. D. Larcher and J. M. Tarascon, *Nat. Chem.*, **7**, 19 (2015).

6. X. Xiang, K. Zhang and J. Chen, *Adv. Mater.*, **27**, 5343 (2015).

7. N. Yabuuchi, K. Kubota, M. Dahbi and S. Komaba, *Chem. Rev.*, **114**, 11636 (2014).

8. Y. Huang, Y. Zheng, X. Li, F. Adams, W. Luo, Y. Huang and L. Hu, *ACS Energy Lett.*, **3**, 1604 (2018).

9. R. J. Clément, P. G. Bruce and C. P. Grey, *J. Electrochem. Soc.*, **162**, A2589 (2015).

10. M. H. Han, E. Gonzalo, G. Singh and T. Rojo, *Energy Environ. Sci.*, **8**, 81 (2015).

11. N. Ortiz-Vitoriano, N. E. Drewett, E. Gonzalo and T. Rojo, *Energy Environ. Sci.*, **10**, 1051 (2017).

12. X. Rong, J. Liu, E. Hu, Y. Liu, Y. Wang, J. Wu, X. Yu, K. Page, Y.-S. Hu, W. Yang, H. Li, X.-Q. Yang, L. Chen and X. Huang, *Joule*, **2**, 1 (2017).

13. J. Xu, D. H. Lee, R. J. Clément, X. Yu, M. Leskes, A. J. Pell, G. Pintacuda, X.-Q.

Yang, C. P. Grey and Y. S. Meng, *Chem. Mater.*, **26**, 1260 (2014).

14. N. Yabuuchi, R. Hara, K. Kubota, J. Paulsen, S. Kumakura and S. Komaba, *J. Mater. Chem. A*, **2**, 16851 (2014).

15. N. Yabuuchi, M. Kajiyama, J. Iwatate, H. Nishikawa, S. Hitomi, R. Okuyama, R. Usui, Y. Yamada and S. Komaba, *Nat. Mater.*, **11**, 512 (2012).

16. M. H. Han, E. Gonzalo, N. Sharma, J. M. López del Amo, M. Armand, M. Avdeev, J. J. Saiz Garitaonandia and T. Rojo, *Chem. Mater.*, **28**, 106 (2016).

17. L. Mu, S. Xu, Y. Li, Y. S. Hu, H. Li, L. Chen and X. Huang, *Adv. Mater.*, **27**, 6928 (2015).

18. L. Liu, X. Li, S.-H. Bo, Y. Wang, H. Chen, N. Twu, D. Wu and G. Ceder, *Adv. Energy Mater.*, **5**, 1500944 (2015).

19. V. Duffort, E. Talaie, R. Black and L. F. Nazar, *Chem. Mater.*, **27**, 2515 (2015).

20. J. M. Paulsen, D. Larcher and J. R. Dahn, *J. Electrochem. Soc.*, **147**, 2862 (2000).

21. Y. Li, Z. Yang, S. Xu, L. Mu, L. Gu, Y.-S. Hu, H. Li and L. Chen, *Adv. Sci.*, **2**, 1500031 (2015).

22. Z. Lu and J. R. Dahn, *J. Electrochem. Soc.*, **148**, A1225 (2001).

23. D. H. Lee, J. Xu and Y. S. Meng, *Phys. Chem. Chem. Phys.*, **15**, 3304 (2013).

24. T. Risthaus, D. Zhou, X. Cao, X. He, B. Qiu, J. Wang, L. Zhang, Z. Liu, E. Paillard, G. Schumacher, M. Winter and J. Li, *J. Power Sources*, **395**, 16 (2018).

25. Y. Liu, X. Fang, A. Zhang, C. Shen, Q. Liu, H. A. Enaya and C. Zhou, *Nano Energy*, **27**, 27 (2016).

26. J. Mao, K. Dai and Y. Zhai, *Electrochim. Acta*, **63**, 381 (2012).

27. K. Dai, J. Mao, Z. Li, Y. Zhai, Z. Wang, X. Song, V. Battaglia and G. Liu, *J. Power Sources*, **248**, 22 (2014).

28. K. Dai, J. Mao, X. Song, V. Battaglia and G. Liu, *J. Power Sources*, **285**, 161 (2015).

29. J. Mao, K. Dai, M. Xuan, G. Shao, R. Qiao, W. Yang, V. S. Battaglia and G. Liu, *ACS Appl. Mater. Interfaces*, **8**, 9116 (2016).

30. J. Mao, M. Ma, P. Liu, J. Hu, G. Shao, V. Battaglia, K. Dai and G. Liu, *Solid State Ionics*, 70 (2016).

31. Q. Liu, Z. Hu, M. Chen, C. Zou, H. Jin, S. Wang, Q. Gu and S. Chou, *J. Mater. Chem. A*, **7**, 9215 (2019).

32. R. Qiao, K. Dai, J. Mao, T.-C. Weng, D. Sokaras, D. Nordlund, X. Song, V. S. Battaglia, Z. Hussain, G. Liu and W. Yang, *Nano Energy*, **16**, 186 (2015).

33. R. Qiao, T. Chin, S. J. Harris, S. Yan and W. Yang, *Curr. Appl. Phys.*, **13**, 544 (2013).

34. R. Qiao, Y. Wang, P. Olalde-Velasco, H. Li, Y.-S. Hu and W. Yang, *J. Power Sources*, **273**, 1120 (2015).

35. Q. Li, R. Qiao, L. A. Wray, J. Chen, Z. Zhuo, Y. Chen, S. Yan, F. Pan, Z. Hussain and W. Yang, *J. Phys. D*, **49**, 413003 (2016).

36. J. Wu, J. Song, K. Dai, Z. Zhuo, L. A. Wray, G. Liu, Z.-x. Shen, R. Zeng, Y. Lu and W. Yang, *J. Am. Chem. Soc.*, **139**, 18358 (2017).

37. K. Dai, J. Wu, Z. Zhuo, Q. Li, S. Sallis, J. Mao, G. Ai, C. Sun, Z. Li, W. E. Gent, W. C. Chueh, Y.-d. Chuang, R. Zeng, Z.-x. Shen, F. Pan, S. Yan, L. F. J. Piper, Z.

Hussain, G. Liu and W. Yang, *Joule*, **3**, 518 (2019).

38. W. Yang, *Nat. Energy*, **3**, 619 (2018).

39. Z. Zhuo, C. D. Pemmaraju, J. Vinson, C. Jia, B. Moritz, I. Lee, S. Sallies, Q. Li, J. Wu, K. Dai, Y.-d. Chuang, Z. Hussain, F. Pan, T. P. Devereaux and W. Yang, *J. Phys. Chem. Lett.*, **9**, 6378 (2018).

40. W. Yang and T. P. Devereaux, *J. Power Sources*, **389**, 188 (2018).

41. M. Doyle, J. Newman and J. Reimers, *J. Power Sources*, **52**, 211 (1994).

42. G. Liu, L. Wen, Y. Li and Y. Kou, *Ionics*, **21**, 1011 (2014).

43. R. Dang, Q. Li, M. Chen, Z. Hu and X. Xiao, *Phys. Chem. Chem. Phys.*, **21**, 314 (2018).

44. C. Heubner, M. Schneider and A. Michaelis, *J. Power Sources*, **307**, 199 (2016).

45. T. Risthaus, J. Wang, A. Friesen, R. Krafft, M. Kolek and J. Li, *J. Electrochem. Soc.*, **163**, A2103 (2016).

46. S. Kuppan, Y. Xu, Y. Liu and G. Chen, *Nat. Commun.*, **8** (2017).

47. Y. Xia and M. Yoshio, *J. Electrochem. Soc.*, **144**, 4186 (1997).

48. T. Zhang, J. Mao, X. Liu, M. Xuan, K. Bi, X. L. Zhang, J. Hu, J. Fan, S. Chen and G. Shao, *Rsc Adv.*, **7**, 41504 (2017).

49. S. Y. Lee, J. H. Kim and Y. C. Kang, *Electrochim. Acta*, **225**, 86 (2017).

Table

Table 1. Comparation of the electrochemical performance between this work and references.

References	Preparation method	Voltage cut-off (V)	Capacity (mAh g^{-1})	Rate (mAh g^{-1})	Capacity fading (% per cycle)	Na^+ diffusion coefficient (cm^2 s^{-1})
Ref.[31]	sol-gel	2.0-4.0	93.0@0.1 C	58.2@20 C	0.025@1 C	$\sim10^{-10}$
Ref.[23]	co-precipitation	2.3-4.1	87@0.1 C	62.4@2 C	0.16@0.2 C	7×10^{-9} – 1×10^{-10}
Ref [43]	solid state	2.5-4.3	101@0.1 C	45@5 C	0.21@0.5 C	$\sim10^{-12}$
Ref.[49]	spray pyrolysis	2.0-4.0	86@0.1 C	81@1 C	0.038@0.1 C	-
Ref.[42]	solid state	2.0-4.0	88.5@0.1 C	77.4@2 C	0.74@0.5 C	-
This work	PVP-combustion	2.3-4.1	87.6@0.1 C	80.2@40 C	0.02@1 C	$\sim10^{-10}$

Fig. 1

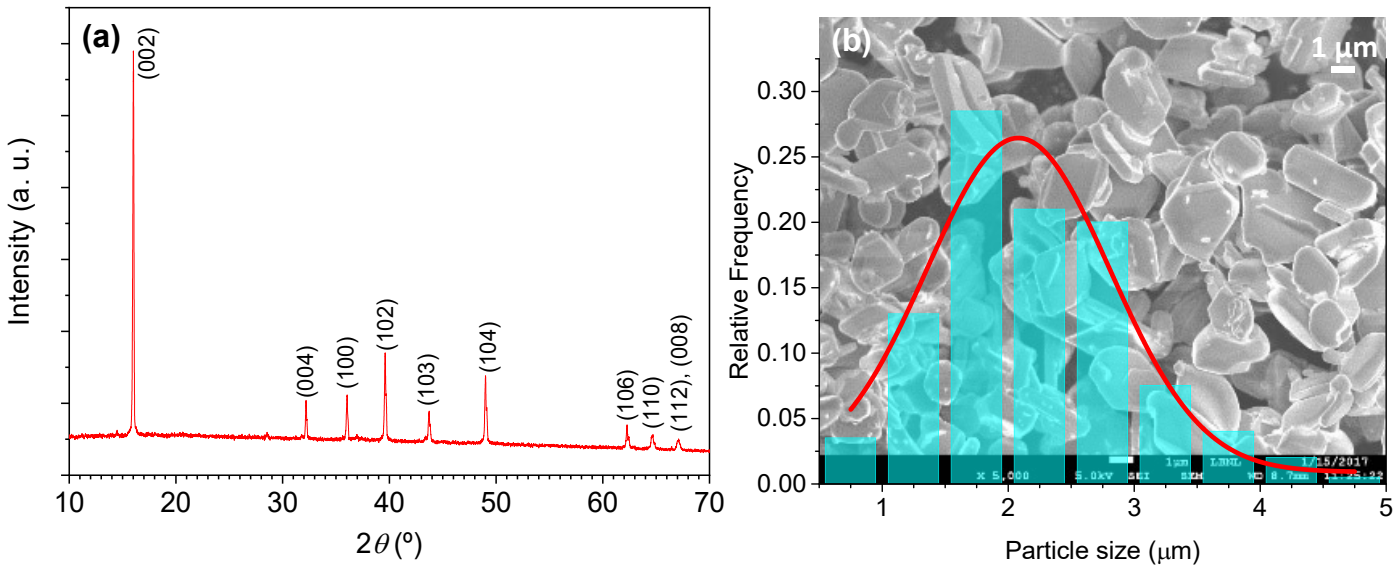

Fig. 1. Morphology and structure of the $Na_{2/3}Ni_{1/3}Mn_{2/3}O_2$. (a) XRD pattern. (b) SEM image and particle size distribution counted from a lower-magnification SEM image.

Fig. 2

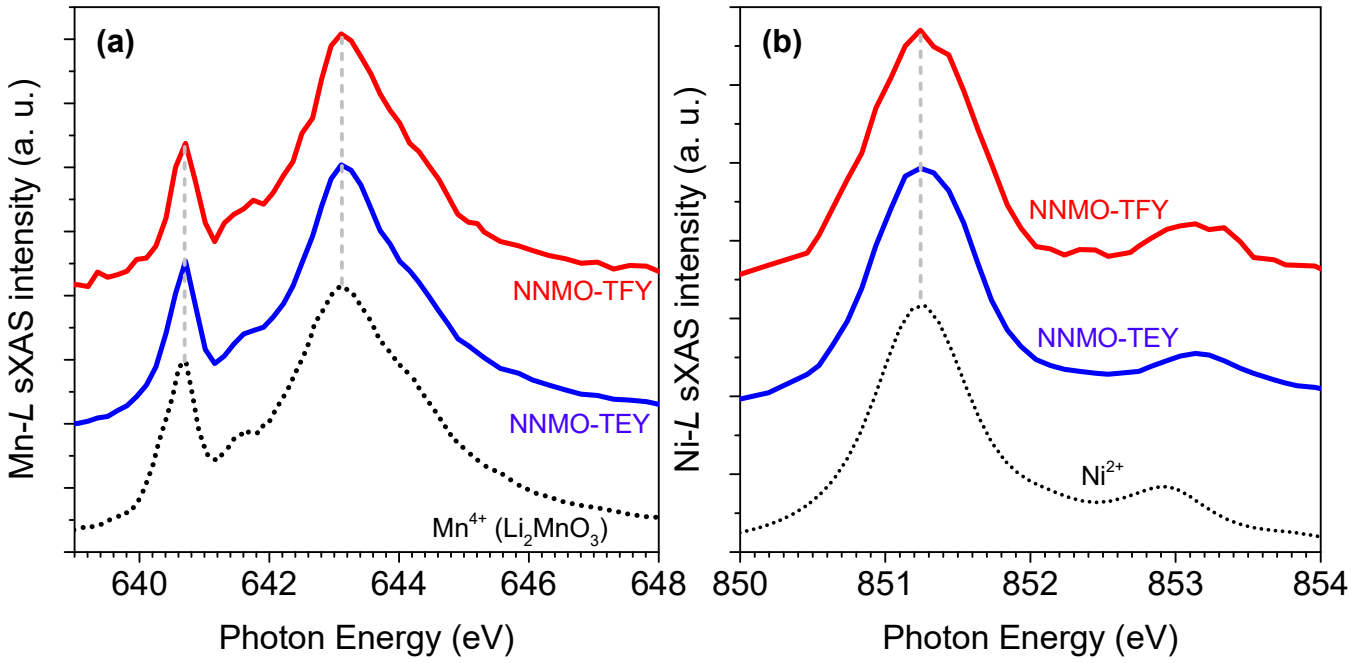

Fig. 2. Soft X-ray absorption spectra of $Na_{2/3}Ni_{1/3}Mn_{2/3}O_2$ associated with standard spectra. (a) Mn L_3-edge. (b) Ni L_3-edge.

Fig. 3

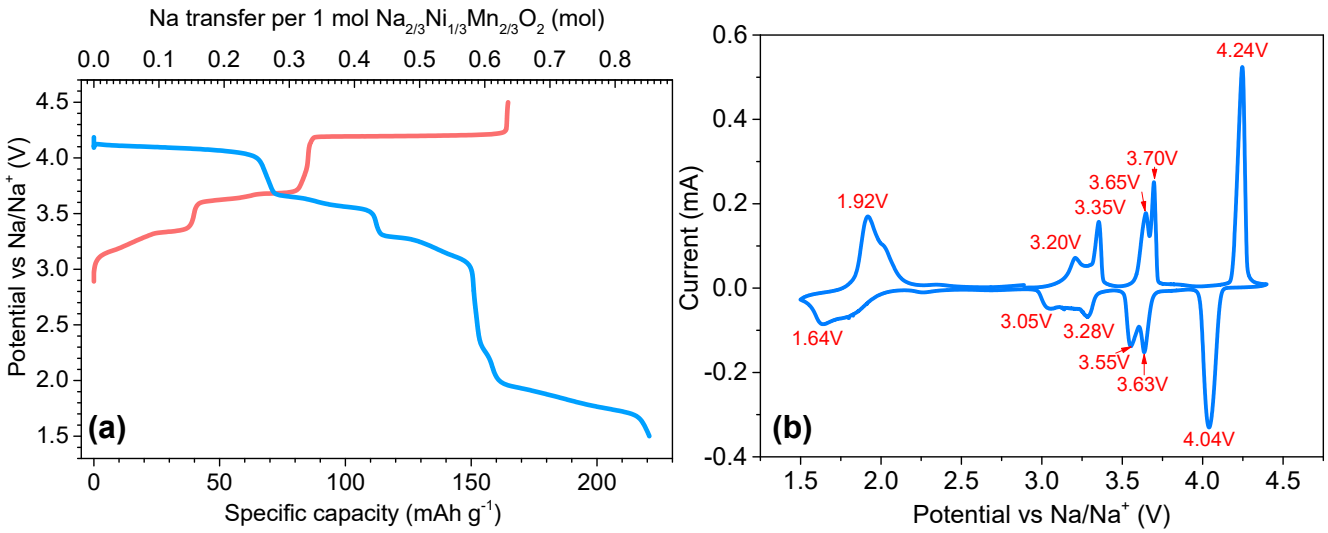

Fig. 3. (a) Voltage profiles of $Na_{2/3}Ni_{1/3}Mn_{2/3}O_2$ during initial charge and discharge process at 0.1 C between 1.5-4.5 V. (b) Cyclic voltammetry curve of $Na_{2/3}Ni_{1/3}Mn_{2/3}O_2$ with a 0.05 mV s^{-1} scan speed.

Fig. 4

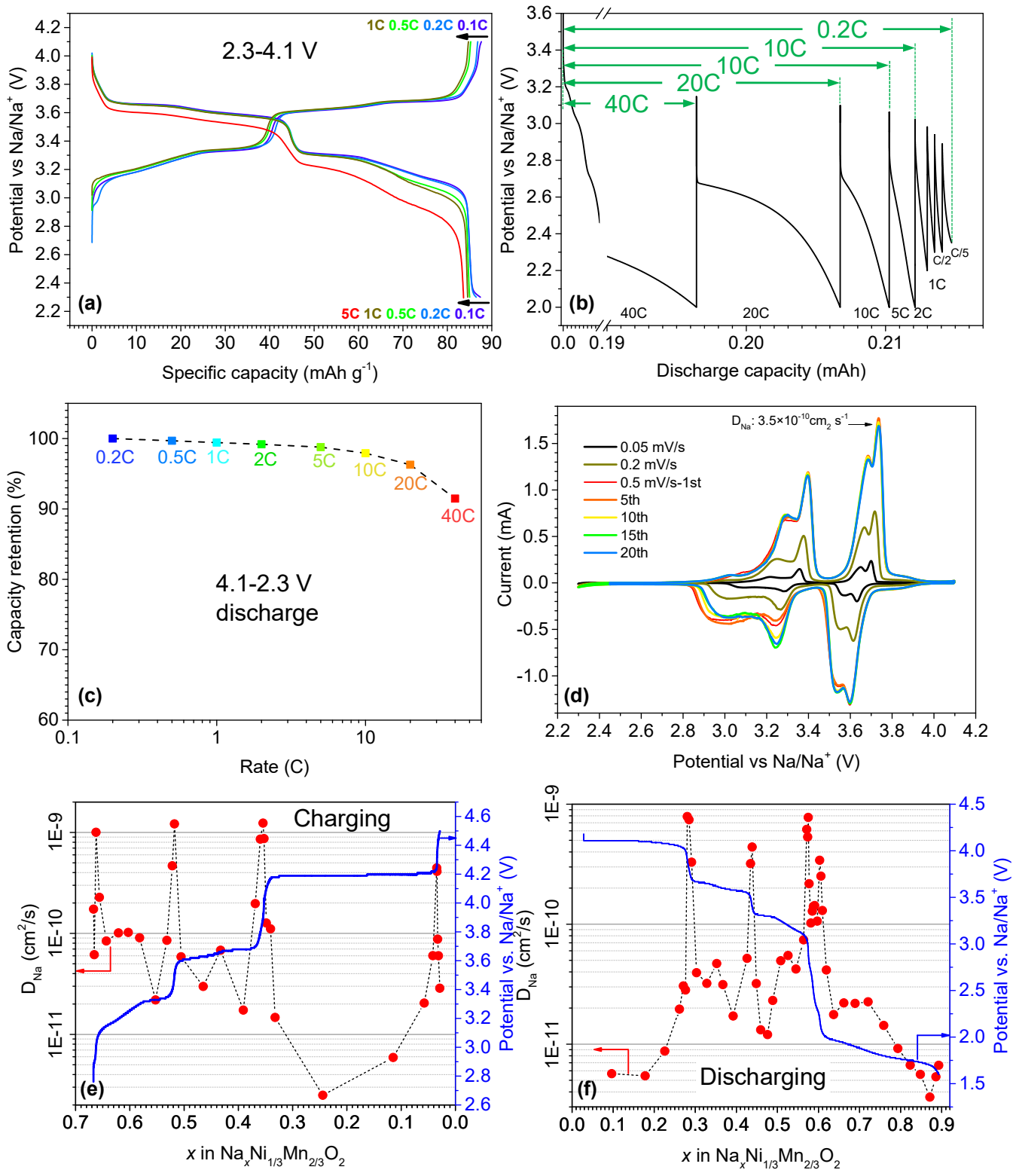

Fig. 4. Rate capability and kinetics of $Na_{2/3}Ni_{1/3}Mn_{2/3}O_2$. (a) The charging and discharging profiles between 2.3-4.1 V at different rates. (b) The discharging profile during fast rate test and diagram of capacity calculation at different rates. (c) The capacity retention at different rates relative to 0.2 C between 2.3-4.1 V during fast rate test. (d) Cyclic voltammetry curves with different scan speed. (e-f) The Na^+ diffusion coefficient measured potentiostatic intermittent titration technique (PITT) tests associated with voltage curves during tests.

Fig. 5

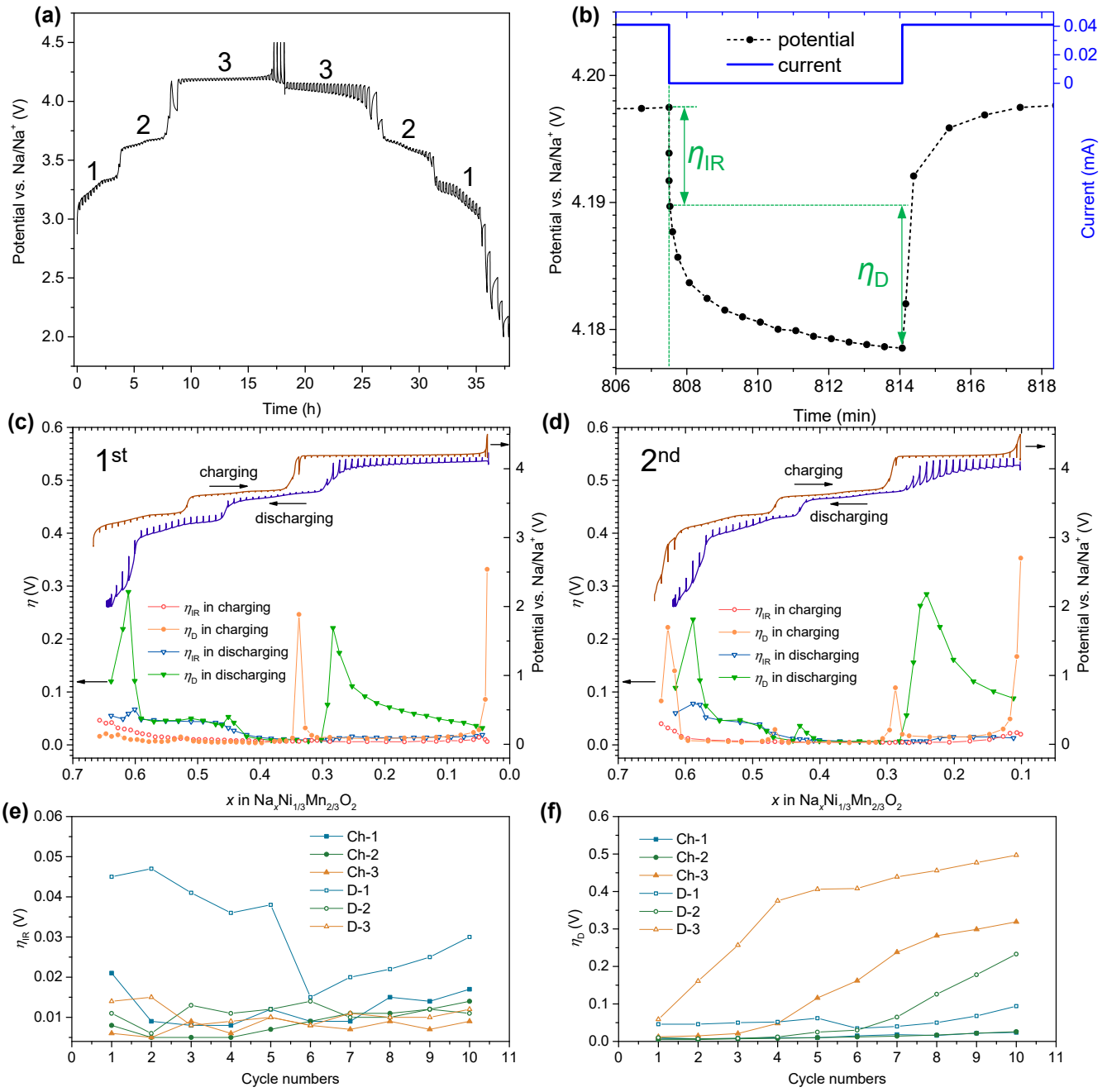

Fig. 5. galvanostatic intermittent titration technique (GITT) tests and overpotentials of $Na_{2/3}Ni_{1/3}Mn_{2/3}O_2$. (a) The charging and discharging profiles vs. time. (b) Diagram of η_{IR} and η_D. (c-d) The overpotentials during GITT tests associated with voltage curves vs Na content in 1st and 2nd cycles. (e) η_{IR} at different plateau in (a) at different cycles. (f) η_D at different plateau in (a) at different cycles.

Fig. 6

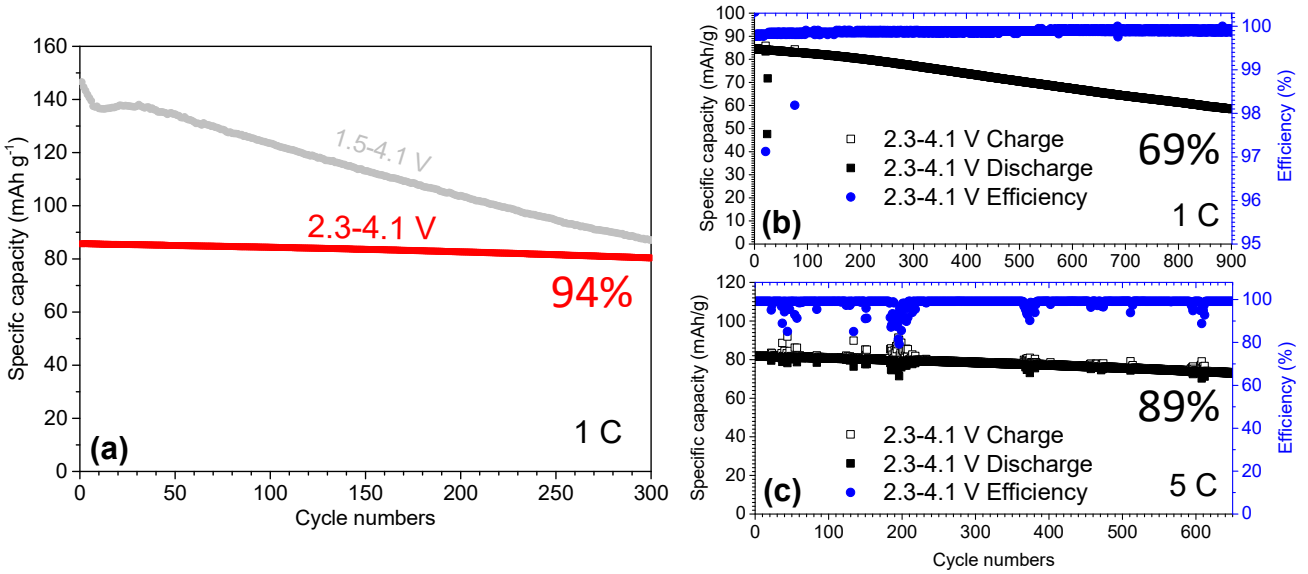

Fig. 6. Cycling stability of $Na_{2/3}Ni_{1/3}Mn_{2/3}O_2$. (a) The discharge capacity vs. cycle numbers between 2.3-4.1 V and 1.5-4.1 V at 1 C. (b) The charge and discharge capacity and coulombic efficiency vs. cycle numbers between 2.3-4.1 at 1 C. (c) The charge and discharge capacity and coulombic efficiency vs. cycle numbers between 2.3-4.1 at 5 C.